Letter Vol. 6, No. 11 / November 2019 / Optica 1412

optica

Spatiotemporal self-similar fiber laser

Uğur Teğin,[1,2,*] Eirini Kakkava,[1] Babak Rahmani,[2] Demetri Psaltis,[1] and Christophe Moser[2]

[1]Optics Laboratory, École Polytechnique Fédérale de Lausanne, Lausanne, Switzerland
[2]Laboratory of Applied Photonics Devices, École Polytechnique Fédérale de Lausanne, Lausanne, Switzerland
*Corresponding author: ugur.tegin@epfl.ch

Received 13 August 2019; revised 7 October 2019; accepted 10 October 2019 (Doc. ID 375350); published 4 November 2019

Spatiotemporal mode-locked fiber lasers are a type of ultrafast lasers for which the longitudinal and transverse modes of the multimode fiber cavities are locked via nonlinear interaction in the cavity. Here we report the experimental realization of a spatiotemporally mode-locked fiber laser with self-similar pulse evolution. The multimode fiber oscillator generates parabolic pulses at 1030 nm with 90 mW average power, a near-Gaussian beam quality ($M^2 \leq 1.4$), and 2.3 ps (192 fs externally dechirped) pulse duration. Numerical simulations confirm the experimental observations of self-similar pulse propagation. These results will enable further investigation of nonlinear dynamics in spatiotemporal mode-locked fiber lasers. © 2019 Optical Society of America under the terms of the OSA Open Access Publishing Agreement

https://doi.org/10.1364/OPTICA.6.001412

For single-mode fiber lasers, ytterbium-based laser systems are generally preferred to achieve high-power pulses with relatively broadband spectra. Over the years, dispersion engineering techniques have been demonstrated to obtain various ultrashort pulse types in ytterbium-based fiber cavities such as soliton pulses [1], dispersion-managed soliton pulses [2] and dispersion-managed self-similar pulses [3]. These pulse types require dispersion mapping inside the cavity. For ytterbium-based fiber lasers, this can be achieved with the bulk grating compressor or dispersion-shifted photonic crystal fibers. In 2006, Chong *et al.* demonstrated the first dissipative soliton pulse formation with an all-normal-dispersion cavity [4]. For ytterbium-based laser systems, all-normal-dispersion cavities provide a simple platform to build all-fiber dissipative soliton lasers [5,6]. The generation of mode-locked dissipative soliton pulses is attributed to spectral intracavity filtering by using 8–12 nm bandpass filters. Interestingly, when the intra-cavity bandpass filter becomes narrow (≤ 4 nm), the temporal pulse shape changes from Gaussian to parabolic [7]. Renninger *et al.* reported this phenomenon in all-normal-dispersion cavity design; with strong spectral filtering, a self-similar pulse can be generated in the gain segment of the laser cavity. These self-similar pulses are referred to as amplifier similariton pulses. Initially, such self-similar pulses based on strong filtering and an amplifier scheme were studied and proposed in fiber amplifiers [8,9] as an alternative to chirped pulse amplification [10]. Moreover, these pulses are a class of solution to the nonlinear Schrödinger equation including a gain term and transform nonlinear phase to a form of linear frequency chirp [8]. The amplifier similariton pulses and their generation mechanism and intracavity propagation behavior are different than dispersion-managed similaritons, which do not require strong spectral filtering and feature a parabolic spectral shape. Compared to dissipative soliton and dispersion-managed similariton pulses, amplifier similaritons experience large spectral breathing (the ratio of spectral bandwidth before and after the spectral filter is >5). This distinctive behavior generates mode-locked pulses with a broader spectrum and hence potentially shorter pulse duration. Because the chirp of the output pulse depends solely on the gain segment, the amplifier similariton pulses also feature less chirp than given by the total cavity dispersion [7]. Recently, Ma *et al.* demonstrated an ytterbium-based all-normal self-similar mode-locked fiber laser tunable from 1030 to 1100 nm by suppressing amplified spontaneous emission by heating the gain fiber [11]. So, far these studies were done in single-mode laser cavities.

In recent years, graded index multimode fibers (GIMFs) have become subject to extensive study due to their unique nonlinear properties and potential higher power handling capacities. With low modal dispersion and periodic self-imaging, spatiotemporal pulse propagation of high-power pulses in GIMF generates interesting nonlinear effects such as spatiotemporal instability [12,13], dispersive wave generation [14], graded-index solitons [15,16], self-beam cleaning [17], nonlinear pulse compression [18], and supercontinuum generation [19,20]. In addition to the aforementioned studies, spatiotemporal mode locking was demonstrated with graded-index multimode fibers in multimode fiber laser cavities by Wright *et al.* [21]. Later, observations of the bound state solitons (soliton molecules) and harmonic mode locking were reported in spatiotemporal mode-locked fiber lasers [22,23]. All of these studies presented laser cavities featuring dissipative soliton pulses with Gaussian temporal profile and low output beam quality. However, to the best of our knowledge, there are no reports on the generation of different temporal pulse types than dissipative solitons in spatiotemporal mode-locked lasers.

Here, we present the first spatiotemporal self-similar fiber laser capable of generating amplifier similariton pulses with a parabolic temporal shape. Interestingly, the train of the mode- locked pulse coming out of the 250 mode GIMF has a stable good beam quality of M^2 value <1.4. The presented laser is an all-normal-dispersion

cavity containing a GIMF with a 50 μm core diameter, a step-index multimode gain, and passive fiber segment, both with a 10 μm core diameter. Mode locking is achieved by nonlinear polarization evolution (NPE) [24]. A narrow bandpass spectral filter with 3.8 nm bandwidth is constructed with a cascade of a bandpass filter with 10 nm bandwidth and a tilted longpass filter. First, numerical simulations are performed to investigate the possibility of amplifier similariton formation in the multimode laser cavity. Encouraged by the numerical simulations, experimental studies were performed with numerically obtained cavity parameters such as the fiber length of each cavity segment. We experimentally achieved self-starting mode locking for which the laser generates amplifier similaritons at 1030 nm with 90 mW average power, 2.4 nJ pulse energy, and 38 MHz repetition rate. The experimental results indicate that the pulse experiences a six-fold increase in its spectral width inside the laser cavity. The chirped output pulse duration is measured as 2.3 ps, which is remarkably short when compared with the group-velocity dispersion of the laser cavity. Both features point to amplifier similariton behavior. The chirped output pulses are externally compressed to 240 fs by a grating pair as measured by a second-order autocorrelation. By reconstructing the pulse profile using the phase and intensity from cross-correlation and spectrum only (PICASO) method [25], we obtained a 172 fs pulse duration with a parabolic temporal shape. The schematic of the fiber laser is illustrated in Fig. 1. The numerical simulations are performed based on this cavity design to investigate the possibility of self-similar pulse formation. We have performed a simulation of spatiotemporal mode locking with the model proposed by Wright *et al.* [21]. A multimode nonlinear Schrödinger equation is solved for the GIMF segment by considering the first six linearly polarized (LP) modes with cylindrical symmetry (more details of simulations can be found in Supplement 1) [26]. A Gaussian intracavity bandpass filter is assumed with 4 nm spectral bandwidth. A stable mode-lock regime is achieved after 30 round-trips as illustrated in Fig. 2. In the gain fiber, a substantial spectral broadening is observed, and after the GIMF segment the spectral bandwidth of the pulse reaches 21.5 nm. This broad spectrum is reduced to 4 nm with a bandpass filter. Thus, the pulse experiences more than 5 times spectral broadening in one round-trip [Fig. 2(b)]. The temporal profile of the pulse is presented in Fig. 2(c), and at output 1 (before the filter) and output 2 (after the filter), pulse durations of 3.3 ps and 1.2 ps are achieved, respectively. As presented in Fig. 2(d), at the end of the gain segment of the cavity, parabolic pulse shape is obtained, which validates the amplifier similariton pulse formation. A numerically obtained beam profile at output 1 is demonstrated in Fig. 2(e). Output 1 and output 2 are the NPE output and the 50:50 output couplers, respectively. For numerical simulations, 2.51 nJ pulse energy is observed at output 1.

The experiments were then performed with the numerically designed cavity. A pump combiner with 10 μm core diameter is integrated to the cavity to couple the 976 nm high-power fiber-coupled diode laser to pump the 1.5 m highly doped ytterbium fiber (nLight Yb-1200-10/125) gain segment. The fiber sections with 10 μm core diameter support three modes at 1 μm. This passive fiber section with 10 μm core diameter is 1.8 m long. In order to excite the higher-order modes of the 250 mode GIMF (Thorlabs GIF50C), the gain fiber is spliced to the 2 m GIMF with a small offset (5 μm). Mode locking was achieved by adjusting the intracavity wave plates. At approximately 1.5 W pump power, self-starting mode locking with a repetition rate of 38 MHz is observed. Experimentally obtained optical spectra and beam profiles from the output couplers before

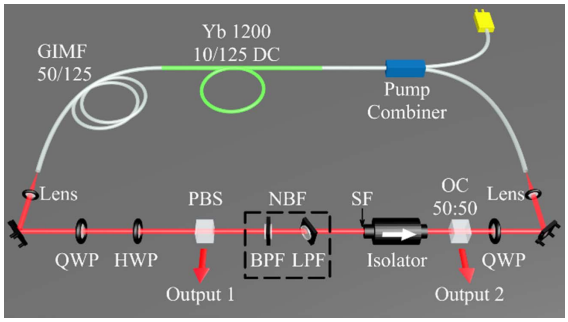

Fig. 1. Schematic of the spatiotemporal self-similar fiber laser: QWP, quarter-wave plate; HWP, half-wave plate; PBS, polarizing beam splitter; NBF, narrow bandpass filter; BPF, bandpass filter; LPF, longpass filter; SF, spatial filter; OC, output coupler; GIMF, graded- index multimode fiber.

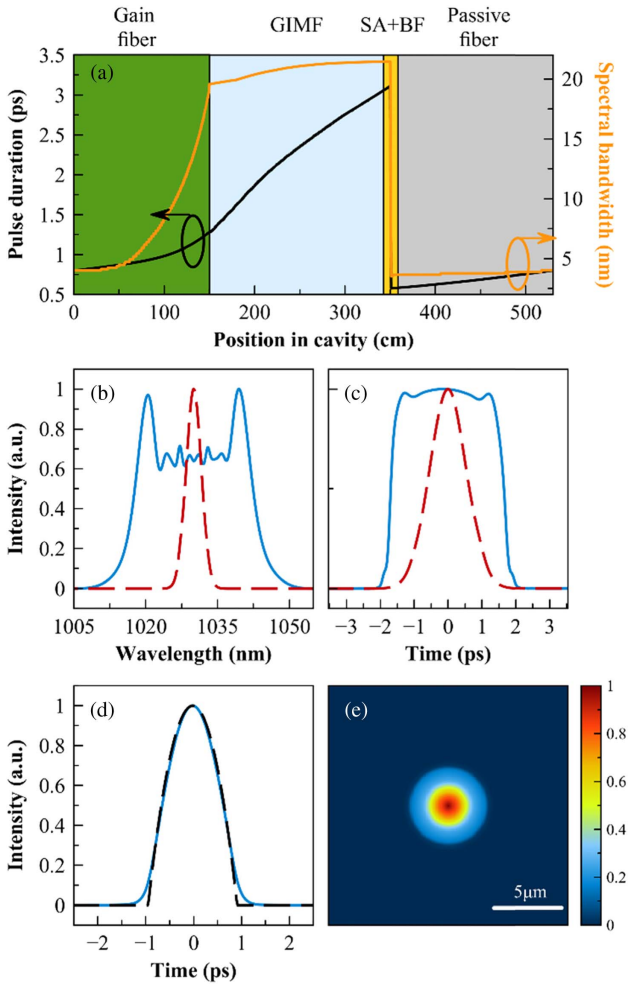

Fig. 2. (a) Simulated pulse duration and spectral bandwidth variation over the cavity: SA, saturable absorber; BF, bandpass filter. (b) Simulated laser spectra and (c) temporal profile obtained at output 1 (solid) and output 2 (dashed). (d) Pulse shape at the end of gain fiber (solid) and theoretical fit with chirp-free parabolic pulse shape (dashed). (e) Numerically obtained beam profile at output 1.

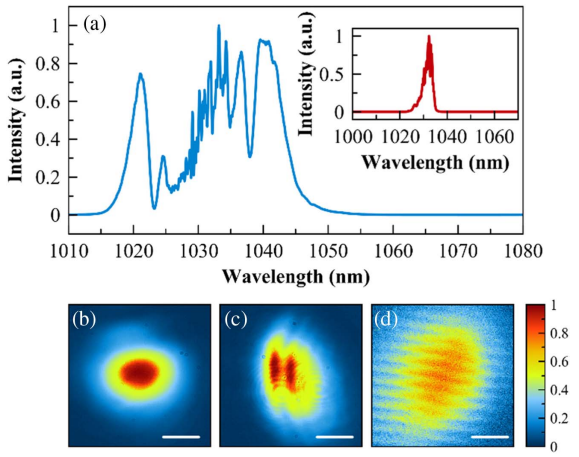

Fig. 3. (a) Measured spectrum from output 1 and output 2 (inset). Measured beam profiles case from (b) output 1 and (c) output 2 for mode-locked operation. (d) Measured spatial beam profile from output 1 for continuous-wave operation case. Scale bars indicated in beam profiles are 520 μm.

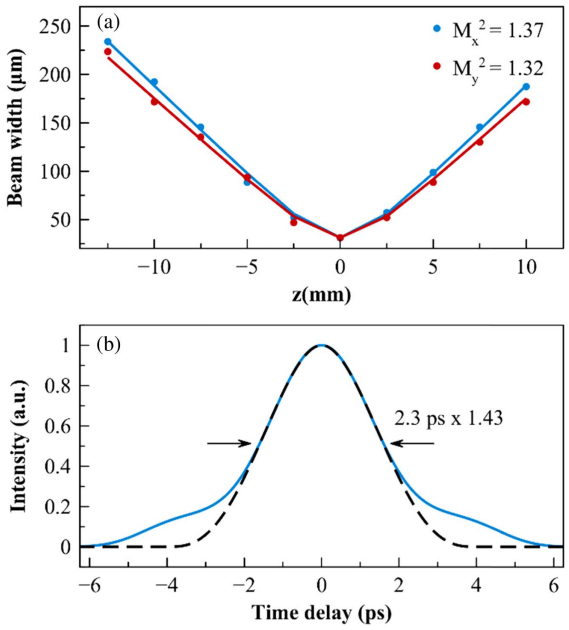

Fig. 4. (a) M^2 measurement of the beam from output 1. (b) Autocorrelation trace of the chirped pulse measured from output 1 (solid) and theoretical fit with chirp-free parabolic pulse shape (dashed).

and after the bandpass filter are presented in Fig. 3. A drastic improvement was observed in the output beam profile when the laser operation changed from continuous-wave to mode-locked operation [see Figs. 3(b) and 3(d)]. The spectral width of the amplifier similariton pulses reached 24 nm after the GIMF, and the spectral profile was reshaped to 3.8 nm with the narrow bandpass filter. This result is consistent with the pulse-breathing ratio of >5 found after one round-trip in a single-mode amplifier similariton laser [7]. The measured output powers of the laser are 90 mW and 10 mW at output 1 and output 2, respectively. After the narrow bandpass intracavity spectral filter, the pulses experience spatial filtering due to the aperture of the isolator [see Fig. 3(a) inset]. We observe that spatial filtering is necessary to achieve spatiotemporal mode locking similarly to dissipative soliton pulses in multimode fiber lasers [21,22]. Beam profiles are measured by a 4f system with 1.5 magnification. As shown in Fig. 3(b), the beam at output port 1, which is immediately after the 250 mode GIMF, has a near-symmetric shape. M^2 measurements are performed to determine the quality of this beam and presented in Fig. 4(a). We experimentally observed a nice beam quality with $M^2 < 1.4$ for the main output (output 1) port of the cavity. For a single-pass propagation configuration Krupa *et al.* presented a drastic improvement in beam profile for a pulse with approximately 1 kW peak power at the end of a 12 m GIMF with a 50 μm core diameter [17]. In our experiment, after the gain segment of the cavity, the peak power of the mode-locked pulses was around 6 kW, which then propagated in a 2 m long GIMF with the same core size. Our simulations indicate that by accumulating every round-trip in a mode-locked cavity, a similar beam cleaning effect is most likely responsible for the clean beam profile we observed. We perform further numerical studies to investigate the evolution of the beam profile inside the GIMF. Single-pass propagation simulations considering 10 LP modes with various initial conditions were simulated, and energy transfer to lower-order modes from higher-order modes was observed. On the other hand, numerical simulations to study the effect of pulse shape on the mode-locked beam quality of the multimode fiber laser were performed as well.

We observed a significant difference in the beam profiles in the simulated dissipative soliton pulses and amplifier similariton pulses. In our studies for various excitation conditions, the amplifier similariton pulses featured more confined spatial energy distribution than the Gaussian pulses. For both studies, more details of the simulations can be found in Supplement 1. The main difference between a Gaussian (dissipative soliton) and parabolic temporal pulse (similariton or amplifier similariton) is that the parabolic pulse shape has more confined temporal energy than the Gaussian pulse (see Visualization 1, Visualization 2, Visualization 3, and Visualization 4). Our simulations show that the more confined temporal distribution translated to a more confined spatial energy distribution at the output of the mode-locked laser and thus better beam quality. Thus, we believe the better beam quality observed in our experiments is due to the generation of amplifier similaritons in the mode-locked multimode laser.

For the pulses from output 1, no secondary pulse formation or periodic oscillation of the pulse train was observed. The duration of the chirped output pulses is 2.3 ps with a 1.43 deconvolution factor as shown in Fig. 4(b). The chirped pulse duration is remarkably smaller for an all-normal-dispersion cavity with total cavity dispersion 0.13 ps^2, and it validates the self-similar behavior of the pulses inside the laser cavity. These pulses are dechirped (compressed) using an external grating compressor with a 300 line/mm diffraction grating pair to 192 fs [Fig. 5(a)]. We utilize the PICASO algorithm to retrieve the temporal profile from the spectrum and autocorrelation data. As presented in Fig. 5(b), the resulting pulse features 172 fs pulse duration with a parabolic temporal profile. We test the power handling capacity of the spatiotemporal self-similar fiber laser by gradually increasing the pump power. Up to 195 mW average power from output port 1, a mode-locked operation with a single pulse on a cavity round-trip, was maintained. This average power was achieved with a 2.1 W pump power level. Pulses yielded 5.1 nJ pulse

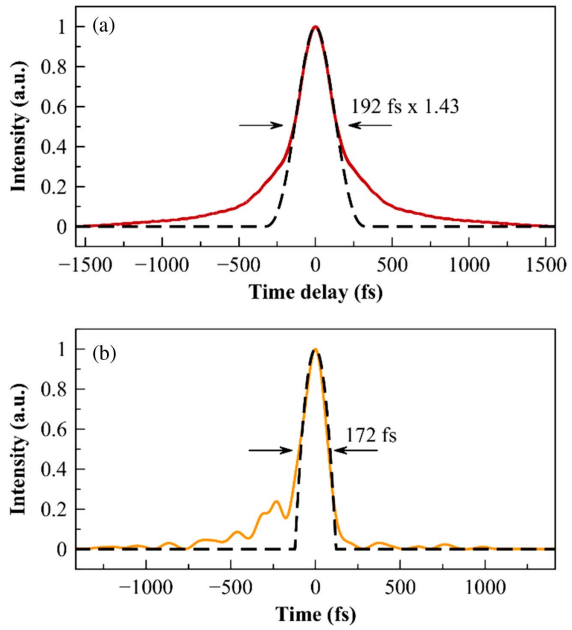

Fig. 5. (a) Autocorrelation trace of the compressed pulse measured from output 1 and theoretical fit with chirp-free parabolic pulse shape (dashed). (b) PICASO-retrieved dechirped pulse shape and parabolic pulse shape fit (dashed).

energy. A broader spectrum (>35 nm) is obtained, but the temporal pulse shape is degraded, and the compressed pulse duration is increased (>300 fs).

In conclusion, we numerically and experimentally demonstrate an all-normal-dispersion ytterbium-based spatiotemporal mode-locked fiber laser supporting self-similar pulse evolution for the first time to our knowledge in the literature. The laser dynamics are numerically and experimentally validated. We obtained intracavity large spectral breathing (>6) and low chirp of the output pulses. Our observations verified the spatiotemporal self-similar pulse formation and the parabolic pulse generation. The oscillator generates amplifier similariton pulses at 1030 nm with 90 mW average power, 2.4 nJ energy, 2.3 ps duration, and 38 MHz repetition rate. Pulses are dechirped to 192 fs via an external grating compressor. Contrary to the beam profile obtained in dissipative multimode mode-locked cavities, we measured a near-Gaussian beam profile of the amplifier similariton pulses with M^2 value <1.4. The combination of good beam quality and sub-200 fs self-similar pulse from a multimode cavity is a promising platform to generate high-power ultrashort pulses. We believe the reported observations are of great interest for nonlinear pulse propagation as well as pulse and beam shaping in spatiotemporal mode-locked fiber lasers. The presented technique can find applications in wavelength and pulse shape tunable laser sources.

Acknowledgment. The authors thank Prof. C. Brès and PHOSL for lending the fiber splicer used in the experiments.

See Supplement 1 for supporting content.

REFERENCES

1. A. Isomäki and O. G. Okhotnikov, Opt. Express **14**, 9238 (2006).
2. B. Ortaç, A. Hideur, T. Chartier, M. Brunel, C. Özkul, and F. Sanchez, Opt. Lett. **28**, 1305 (2003).
3. F. Ilday, J. Buckley, W. Clark, and F. Wise, Phys. Rev. Lett. **92**, 213902 (2004).
4. A. Chong, J. Buckley, W. Renninger, and F. Wise, Opt. Express **14**, 10095 (2006).
5. K. Özgören and F. Ilday, Opt. Lett. **35**, 1296 (2010).
6. U. Teğin and B. Ortaç, Opt. Lett. **43**, 1611 (2018).
7. W. H. Renninger, A. Chong, and F. W. Wise, Phys. Rev. A **82**, 021805 (2010).
8. M. Fermann, V. Kruglov, B. Thomsen, J. Dudley, and J. Harvey, Phys. Rev. Lett. **84**, 6010 (2000).
9. V. Kruglov, A. Peacock, J. Dudley, and J. Harvey, Opt. Lett. **25**, 1753 (2000).
10. D. Strickland and G. Mourou, Opt. Commun. **55**, 447 (1985).
11. C. Ma, A. Khanolkar, and A. Chong, Opt. Lett. **44**, 1234 (2019).
12. K. Krupa, A. Tonello, A. Barthélémy, V. Couderc, B. M. Shalaby, A. Bendahmane, G. Millot, and S. Wabnitz, Phys. Rev. Lett. **116**, 183901 (2016).
13. U. Teğin and B. Ortaç, IEEE Photon. Technol. Lett. **29**, 2195 (2017).
14. L. G. Wright, D. N. Christodoulides, and F. W. Wise, Nat. Photonics **9**, 306 (2015).
15. W. H. Renninger and F. W. Wise, Nat. Commun. **4**, 1719 (2013).
16. A. S. Ahsan and G. P. Agrawal, Opt. Lett. **43**, 3345 (2018).
17. K. Krupa, A. Tonello, B. M. Shalaby, M. Fabert, A. Barthélémy, G. Millot, S. Wabnitz, and V. Couderc, Nat. Photonics **11**, 237 (2017).
18. K. Krupa, A. Tonello, V. Couderc, A. Barthélémy, G. Millot, D. Modotto, and S. Wabnitz, Phys. Rev. A **97**, 043836 (2018).
19. G. Lopez-Galmiche, Z. S. Eznaveh, M. Eftekhar, J. A. Lopez, L. Wright, F. Wise, D. Christodoulides, and R. A. Correa, Opt. Lett. **41**, 2553 (2016).
20. U. Teğin and B. Ortaç, Sci. Rep. **8**, 12470 (2018).
21. L. G. Wright, D. N. Christodoulides, and F. W. Wise, Science **358**, 94 (2017).
22. H. Qin, X. Xiao, P. Wang, and C. Yang, Opt. Lett. **43**, 1982 (2018).
23. Y. Ding, X. Xiao, P. Wang, and C. Yang, Opt. Express **27**, 11435 (2019).
24. M. Hofer, M. Ober, F. Haberl, and M. Fermann, IEEE J. Quantum Electron. **28**, 720 (1992).
25. J. Nicholson, J. Jasapara, W. Rudolph, F. Omenetto, and A. Taylor, Opt. Lett. **24**, 1774 (1999).
26. A. Mafi, J. Lightwave Technol. **30**, 2803 (2012).

128.178.141.47 (a) 2022-12-14 11:03:02)